EPR and optical absorption of Fe^{+}, Fe^{2+}, Fe^{3+}, and Fe^{4+} on tetragonal sites in $CdSiP_2$

U. Kaufmann

Institut für Angewandte Festkörperphysik der Fraunhofer-Gesellschaft, D-7800 Freiburg, Federal Republic of Germany

(Received 12 April 1976)

An EPR investigation of $CdSiP_2$:Fe reveals the presence of substitutional, photosensitive Fe^{+}, Fe^{2+}, Fe^{3+}, and Fe^{4+} impurities, each charge state being associated with a highly anisotropic EPR spectrum. The non-Kramers ions Fe^{2+} and Fe^{4+} are still observable at 300 K. At 20 K all Fe centers, except Fe^{+}, exhibit a well-resolved phosphorus ligand hyperfine splitting. The anisotropy of this splitting is used to demonstrate the magnetic inequivalence of the two Si sites in $CdSiP_2$. For Fe^{2+} and Fe^{4+} a complete analysis of the $S = 2$ spin Hamiltonian is possible. Near-ir absorption bands due to Fe^{2+} and Fe^{4+} are observed. A correlation with the EPR results allows the determination of the crystal-field parameters Dq, Ds, and Dt. Static crystal-field theory, supplemented to include covalency effects, according to the model of Vallin and Watkins, accounts satisfactorily for all experimental results, except for the EPR data of Fe^{4+}. It is suggested that this discrepancy is due to covalent effects beyond those explicitly considered.

I. INTRODUCTION

Ternary semiconductors of type I_B-III-VI_2 and II_B-IV-V_2 have received much interest because of their applicability in optoelectronic and nonlinear optical devices.[1] From a more fundamental point of view they are suitable hosts for the study of defects in a noncubic environment, the site symmetry at both metal sites being S_4. These materials crystallize in the tetragonal chalcopyrite structure and one may look at them as the ternary analogs of the zinc-blende II-VI and III-V compounds. $CdSiP_2$, for instance, can be viewed to originate from GaP by an ordered substitution of Ga by Cd and Si.

Transition-metal ions, which are often encountered as trace impurities in ternary semiconductors, form deep levels and these can strongly affect the optical[2] and electrical[3] properties. This paper presents a detailed electron-paramagnetic-resonance (EPR) and optical analysis of iron impurities in $CdSiP_2$. The most prominent EPR signals observed in nominally pure $CdSiP_2$ were found to be induced by iron contaminations. A careful investigation of intentionally doped crystals revealed the presence of four photosensitive substitutional iron centers which were identified as $Fe^{+}(d^7)$, $Fe^{2+}(d^6)$, $Fe^{3+}(d^5)$, and $Fe^{4+}(d^4)$. Fe^{2+} and Fe^{4+} are non-Kramers ions which are usually difficult to detect by EPR. It is remarkable that their EPR spectra in $CdSiP_2$ are still observable at room temperature with relatively narrow linewidths. At low temperatures all iron centers, except Fe^{+}, display a well-resolved phosphorus ligand hyperfine (hf) splitting. It is possible to demonstrate the inequivalence of the two group-IV sites in the unit cell of a II_B-IV-V_2 compound via the anisotropy of this ligand hf splitting. The experimental data are interpreted in the framework of static-crystal-field theory. Covalency effects are taken into account as in the treatment of Vallin and Watkins.[4]

Most EPR experiments were performed on a conventional VARIAN 35-GHz spectrometer covering a field range of 25 kG. A few EPR spectra were also recorded at 9.5 GHz. The setup for the optical absorption measurements has been described elsewhere.[5]

All $CdSiP_2$ samples used in this study have been grown by the chemical-transport method using iodine as transporting agent. The nominal iron concentrations were $\approx$1000 ppm. Several not intentionally doped crystals were supplied to us by Professor R. Nitsche. Their iron impurity content is estimated to be one to two orders of magnitude smaller than that of our doped crystals.

II. EXPERIMENTAL RESULTS AND ASSIGNMENTS

A. EPR results

1. Fe^{2+} and Fe^{4+}

Figure 1 shows an over-all EPR spectrum of iron-doped $CdSiP_2$ with the static magnetic field H parallel to the c axis. EPR lines marked with an asterisk are only observable if the sample is irradiated with visible or uv light *in situ*. If H is not exactly along c, additional lines corresponding to "forbidden" transitions become visible. Their extrapolated position is indicated by arrows in Fig. 1.

The $Fe^{2+}(S = 2)$ spectrum for $\vec{H} \| \vec{c}$ consists of two lines at $H \approx 2.6$ (width ≈ 110 G) and ≈ 6.2 kG, corresponding to the $2 \longleftrightarrow -2$ and $1 \longleftrightarrow -1$ transition within the $^5\hat{A}$ ground state.[6,7] The intensity of the latter transition decreases if H approaches the c

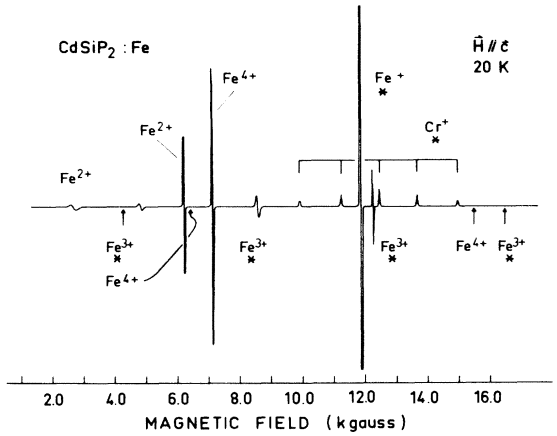

FIG. 1. Over-all EPR spectrum of Fe-doped $CdSiP_2$ recorded at $\nu = 34.8$ GHz. See text for explanations.

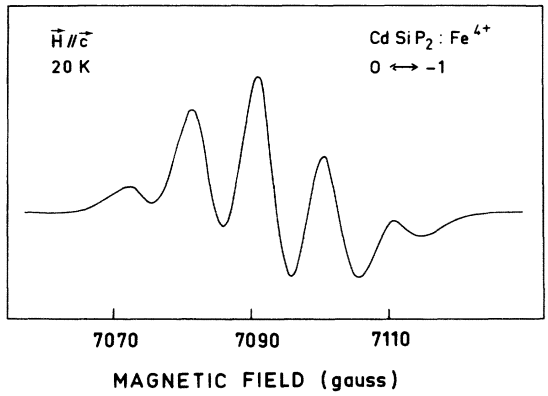

FIG. 3. Ligand hf splitting of the $0 \longleftrightarrow -1$ fine-structure transition of Fe^{4+} arising from interaction with the four nearest-neighbor phosphorus nuclei.

axis but it does *not* vanish for $\vec{H} \| \vec{c}$ in contrast to the corresponding line of Fe^{4+}. Its effective $g_{\|}$ factor is found to be equal at 34.8 and 9.5 GHz. The angular dependence upon rotating H in a (110) plane is shown in Fig. 2. If H is rotated in a (001) plane, the $1 \longleftrightarrow -1$ transition exhibits a cubic anisotropy with an amplitude of 60 ± 20 G.

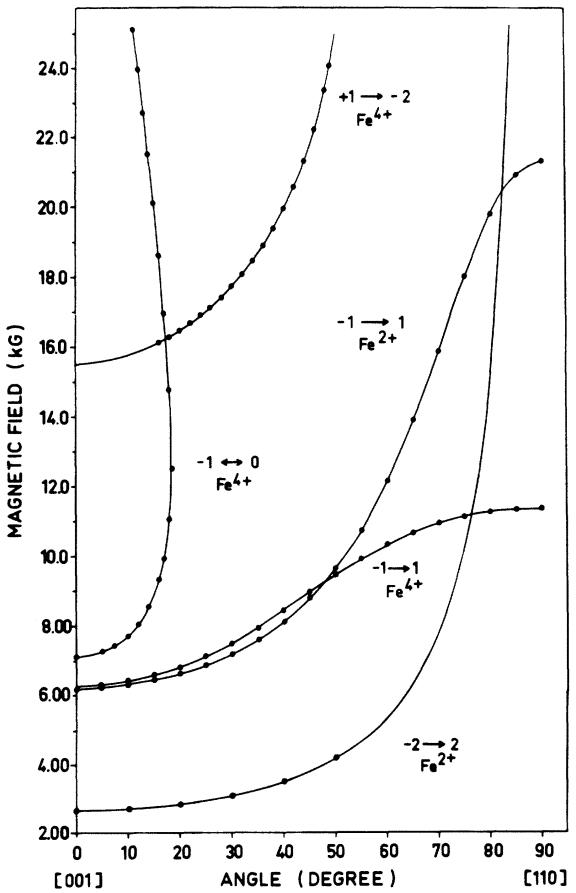

FIG. 2. Angular dependence of observed Fe^{2+} and Fe^{4+} EPR transitions in $CdSiP_2$. The full lines are a computer fit to the experimental points. $T = 20$ K, $\nu = 34.8$ GHz.

The $Fe^{4+}(S = 2)$ spectrum consists of three lines which for $\vec{H} \| \vec{c}$ lie near 6.3, 7.1, and 15.5 kG. They are assigned to the $1 \longleftrightarrow -1$, $0 \longleftrightarrow -1$, and $1 \longleftrightarrow -2$ transitions of the ${}^5\hat{B}^b$ ground state. Their angular dependence is included in Fig. 2. Under $\vec{H} \perp \vec{c}$ the $1 \longleftrightarrow -1$ transition also shows a weak cubic anisotropy of 15 ± 7 G.

If H is parallel to c or close to it the lines $-1 \longleftrightarrow 1$ Fe^{2+}, $-1 \longleftrightarrow 1$ Fe^{4+}, and $0 \longleftrightarrow -1$ Fe^{4+} display a well-resolved phosphorus ligand hf splitting into five components each having a width of ≈ 5 G, see Fig. 3. Under $\vec{H} \perp \vec{c}$ the $1 \longleftrightarrow -1$ line of Fe^{4+} exhibits ligand hf structure, too. However, the splitting is well resolved only if H makes an angle of $\pm(14 \pm 0.8)^\circ$ with either the positive or negative a or b axis. The Fe^{4+} as well as the Fe^{2+} intensity is slightly reduced by uv irradiation. Spin-Hamiltonian parameters of Fe^{2+} and Fe^{4+} are listed in Table I.

The Fe^{2+} and the Fe^{4+} spectra are still visible at 300 K. The $0 \longleftrightarrow -1$ line of Fe^{4+} has shifted about 300 G to lower fields as compared to the $\vec{H} \| \vec{c}$ spectrum at 20 K and the ligand hf splitting is no longer resolved. However, its width is still only ≈ 27 G. This is quite a remarkable feature for a fine-structure transition of a non-Kramers ion. For comparison, the corresponding line of Cr^{2+} in[4] CdTe has a width of about 350 G at 20 K and broadens beyond detection at higher temperatures.

2. *Fe^{+} and Fe^{3+}*

The Fe^{+} ($S = \frac{3}{2}$) spectrum consists of a single line with $g_{\|} \approx 2.1$ and an effective $g_{\perp}$ factor $g'_{\perp} \approx 4.3$. The values of $g'_{\perp}$ determined at 34.8 and

TABLE I. Ground-state spin-Hamiltonian parameters of Fe^{2+} and Fe^{4+} in $CdSiP_2$ as obtained at $\nu = 34.8$ GHz and $T = 20$ K. Energies are given in cm^{-1}. Calculated values are given in parentheses.

	$g_{\parallel}$	$g_{\perp}$	D [a]	$a+\frac{2}{3}F$	a	$\lvert T_{001}\rvert$ [b]
$^5\hat{A}$ (Fe^{2+})	2.003 (2.002)	2.12 (2.11)	9.9 (10.3)		−0.602 (−0.33)	7.6 [c]
$^5\hat{B}^b$ (Fe^{4+})	1.980	1.997	1.822	0.005	−0.03 ±0.01	8.9 [d]

[a] Sign not determined in the experiment.
[b] In units of 10^{-4} cm^{-1}.
[c] $1 \longleftrightarrow -1$ transition.
[d] $0 \longleftrightarrow -1$ transition.

9.5 GHz were found to be identical. As already mentioned the Fe^+ signal is not observed if the sample is cooled down in the dark. However, once created by uv irradiation, it is the dominant EPR signal and it goes off scale in Fig. 1. Subsequent irradiation with ir light ($\lambda > 1$ μm) quenches the signal almost totally.

Fe^+ was also observed in the isomorphous compound $ZnSiP_2$ and we quote the results here for comparison. As for $CdSiP_2$ only a single line is observed. The EPR parameters determined from measurements at 34.8 and 9.5 GHz are: $g_{\parallel} = 2.113$, $g_{\perp} = 2.134$, and $|2D| = 4.3$ cm^{-1}.

There are four lines in Fig. 1 which can be assigned to Fe^{3+} ($S = \frac{5}{2}$): The lines at ≈ 8.6 and 12.3 kG corresponding to the allowed $-\frac{3}{2} \longleftrightarrow -\frac{1}{2}$ and $\frac{1}{2} \longleftrightarrow -\frac{1}{2}$ transitions and the lines at ≈ 4.2 and 16.5 kG arising from the "forbidden" $\pm\frac{1}{2} \longleftrightarrow \mp\frac{3}{2}$ transitions. For $\vec{H} \| \vec{c}$ the $\frac{1}{2} \longleftrightarrow -\frac{1}{2}$ line is split into five ligand hf components similar to Fe^{2+} and Fe^{4+}. Its effective $g_{\perp}$ factor is $g'_{\perp} = 5.613$ at 34.8 GHz. Irradiation with ir reduces the Fe^{3+} intensity by roughly a factor of 2. Spin-Hamiltonian parameters of Fe^{3+} and Fe^+ are listed in Table II.

The weak saturated quintet of lines in Fig. 1 is probably due to Cr^+ impurities. It is unlikely that this signal is due to Fe since it is weaker in the Fe-doped samples than in nominally pure ones. We merely quote its parameters here and note that g and a are similar to Cr^+ in[8] ZnS: $g = 1.998 \pm 0.003$, $D = \pm (577 \pm 8) \times 10^{-4}$ cm^{-1}, $(a + \frac{2}{3}F) = \mp(0.8 \pm 0.7) \times 10^{-4}$ cm^{-1}, and $|a| = (5.8 \pm 0.7) \times 10^{-4}$ cm^{-1}. In addition to the lines shown in Fig. 1 we observe a photosensitive ligand hf pattern with an *even* number of lines (at least eight) centered near $g \approx 2$. The origin of this signal has not been established.

B. Near-ir absorption

Between 1.0 and 3.0 μm we observe two absorption bands near 1.1 and 1.8 μm in Fe-doped $CdSiP_2$. The latter band is shown in Fig. 4 for $\vec{E} \| \vec{c}$. It is completely polarized, no sharp lines being visible if $\vec{E} \perp \vec{c}$. On the long-wavelength side there are three zero-phonon lines (ZPL) two of which are "hot bands." Note that these hot bands lie 9.1 cm^{-1} and 35.9 ($\approx 4 \times 9.1$) cm^{-1} below the 5334.9-cm^{-1} ZPL. The ZPL's are followed by a series of sidebands some of which can be explained as zone-center phonons.[9] This absorption band is assigned to the $^5\hat{A} \longleftrightarrow {}^5\hat{B}^b$ crystal-field transition of Fe^{2+}.

The band near 1.1 μm is at least one order of magnitude weaker than that at 1.8 μm in all crystals studied, the intensity ratio being variable for crystals from different growth runs. This band also is only observed for $\vec{E} \| \vec{c}$. Two ZPL's at 9264.2 and 9258.8 cm^{-1} are observed, the latter again being a hot band. Their phonon sidebands are very similar to those in the 1.8-μm band. This absorption can be consistently assigned to the $^5\hat{B}^b \rightarrow {}^5\hat{A}$ transition of Fe^{4+}.

III. CRYSTAL-FIELD THEORY OF Fe^{2+} AND Fe^{4+}

A. Level scheme

In a tetragonally distorted tetrahedral environment the free-ion ground state ^5D of Fe^{2+} is split by the action of the cubic field V_{cub}, the axial field V_{tig}, spin-orbit H_{so}, and spin-spin interaction H_{ss} as shown in Fig. 5. The Hamiltonian corresponding

TABLE II. Ground-state spin-Hamiltonian parameters of Fe^+ and Fe^{3+} in $CdSiP_2$.

	$g_{\parallel}$	$g_{\perp}$	$g'_{\perp}$	$2D$ [b]	$\lvert T_{001}\rvert$ [d]
Fe^+	2.097	2.189	4.379	+14 [c]	< 6.5
Fe^{3+}	2.036		5.613 [a]	±1.97 ±0.03	10.8

[a] $\frac{1}{2} \longleftrightarrow -\frac{1}{2}$ transition at 34.8 GHz.
[b] In cm^{-1}.
[c] Calculated from Eq. (21).
[d] In 10^{-4} cm^{-1}.

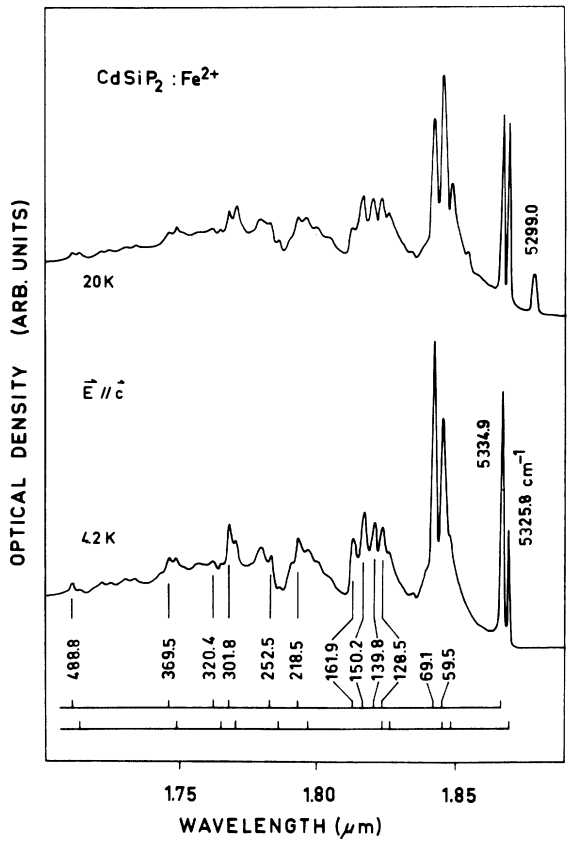

FIG. 4. $^5\hat{A} \rightarrow {}^5\hat{B}^b$ absorption band of Fe^{2+}. No absorption is visible for $\vec{E} \perp \vec{c}$. The separations of the phonon sidebands from the ZPL's are indicated in wave numbers.

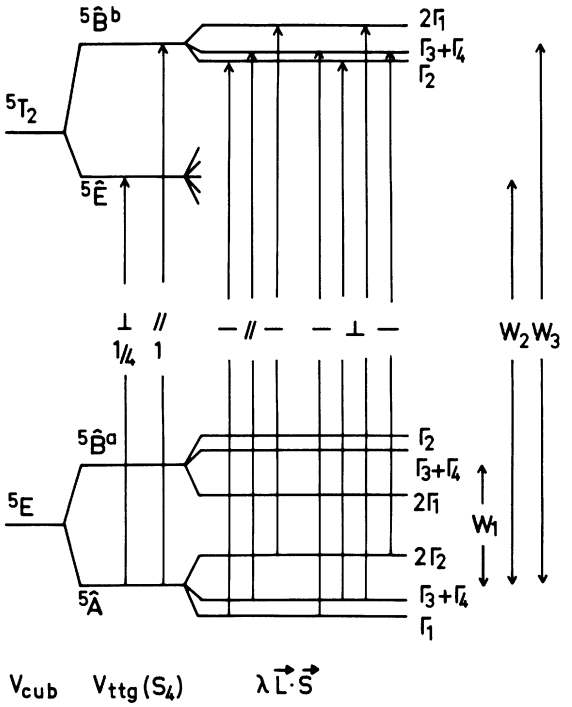

FIG. 5. Crystal-field levels originating from the free-ion ^5D state of Fe^{2+} in a tetragonally distorted tetrahedral environment. The Fe^{4+} level scheme is obtained from this figure by inverting the cubic field splitting and both axial-field splittings. Splittings are not to scale.

to this problem has the form

$$H = V_{\text{cub}} + V_{\text{ttg}} + H_{\text{so}} + H_{\text{ss}} \ . \tag{1}$$

For V_{ttg} we adopt the definition of Vallin *et al.*[10] The axial field splittings of ^5E and $^5T_2$ are denoted by μ and δ, respectively. The signs of μ and δ are defined positive if $^5\hat{B}^a$ and $^5\hat{B}^b$ lie below $^5\hat{A}$ and $^5\hat{E}$, respectively.[11] Within ^5D, H_{so} and H_{ss} can be represented by[12]

$$H_{\text{so}} = \lambda \vec{L} \cdot \vec{S} \ , \tag{2}$$

$$H_{\text{ss}} = -\rho[(\vec{L} \cdot \vec{S})^2 + \tfrac{1}{2}\vec{L} \cdot \vec{S} - \tfrac{1}{3}\vec{L}^2 \vec{S}^2] \ , \tag{3}$$

with $L = S = 2$. Here ρ contains contributions from first-order spin-spin and second-order spin-orbit coupling to excited triplet states of $3d^6$.[13] Only $^5\hat{E}$ exhibits a first-order spin-orbit splitting.

If a magnetic field is applied to the crystal, the Zeeman term

$$H_z = \mu_B k \vec{L} \cdot \vec{H} + g_e \mu_B \vec{S} \cdot \vec{H} \tag{4}$$

must be added to H of Eq. (1). The quantity k is a covalency reduction factor and g_e (= 2.0023) is the free-electron g factor.

The electron configuration of Fe^{4+}, $3d^4$, is complementary to that of Fe^{2+}, $3d^6$. The splitting of the free-ion ground state ^5D of Fe^{4+} is thus obtained from that in Fig. 5 by inverting the cubic-field splitting as well as both axial field splittings. This leaves $^5\hat{B}^b$ as the lowest and $^5\hat{A}$ as the highest state.

We now estimate the parameters λ, k, and ρ which will be needed later. For this purpose it is a good approximation to assume that the radial functions of ^5E and $^5T_2$ are not significantly altered by the tetragonal part of the crystal field.

Within ^5D there are then two reduced matrix elements of the spin-orbit interaction, $\lambda_1 = \langle T_2 || H_{\text{so}} || T_2 \rangle$ and $\lambda_2 = \langle E || H_{\text{so}} || T_2 \rangle$. According to the ligand-field treatment of Vallin and Watkins[4] they are given by

$$\lambda_1 = \lambda_0(1 - K), \quad \lambda_2 = \lambda_0(1 - \tfrac{1}{8}K) \ , \tag{5}$$

where λ_0 is the spin-orbit parameter of the free ion and K is given by $K = K_0\, \zeta/\zeta_d$. Here ζ is the spin-orbit parameter of the ligands (= 299 cm^{-1} for P) and $\zeta^d = 2S|\lambda_0|$. The parameter K_0 is a measure of covalency. In the II-VI compounds it was found to be about 0.13.[4] The spin-orbit parameters λ_1 and λ_2 calculated with this value are listed

TABLE III. Spin-orbit and spin-spin parameters (in cm^{-1}) and covalency reduction factors for iron in $CdSiP_2$.

	λ_0 [a]	λ_1 [b]	λ_2 [b]	k_1 [c]	k_2 [c]	ρ [d]
Fe^{+}	−119	−106	−117	0.60–0.65	0.75–0.80	
Fe^{2+}	−103	−93	−102	0.60–0.65	0.75–0.80	0.83
Fe^{4+}	129	119	128	0.60–0.65	0.75–0.80	1.10

[a] Reference 12.
[b] Calculated from Eqs. (5).
[c] Estimated from Ni^{+} data in I_B-III-S_2 compounds (Ref. 14).
[d] Calculated average of Eqs. (6).

in Table III. In the more covalent phosphorus environment K_0 could be slightly larger. This would reduce λ_1 and λ_2 somewhat below the values quoted in Table III. An additional but small reduction of λ_1 and λ_2 could arise from d-p mixing. In analogy to λ the covalency reduction factor k can take two values, k_1 and k_2. From comparison with ternary sulfides, e.g., $CuGaS_2$, we expect k_1 and k_2 to be in the ranges 0.60–0.65 and 0.75–0.80,[14] respectively.

By symmetry the spin-spin coupling constant ρ can take four values within ^5D. They are given by[4,15]

$$\begin{aligned}
\rho_1 &= (5/9E)(\lambda_1^2 + 2\lambda_2^2) + \rho_{10}\,,\\
\rho_2 &= (5/3E)\lambda_1\lambda_2 + \rho_{20}\,,\\
\rho_3 &= (5/9E)(-\lambda_1^2 + 4\lambda_2^2) + \rho_{30}\,,\\
\rho_4 &= (5/3E)\lambda_2^2 + \rho_{40}\,.
\end{aligned} \tag{6}$$

The first term in these expressions comes from the second-order spin-orbit contribution to ρ, E being an average energy of the excited d^4 (or d^6) triplet states above the quintet ground state.[4] The second term represents the true spin-spin part which for the free Fe^{2+} and Fe^{4+} ion is given by 0.18 and 0.25 cm^{-1},[12] respectively. Using $E \approx 30\,000$ cm^{-1},[16] Eqs. (6) yield ρ values between 1.05 and 1.15 cm^{-1} if we allow for a 20% reduction of ρ_0 from the free-ion value and neglect its cubic anisotropy. Since the anisotropy in ρ is quite small an isotropic average of 1.10 cm^{-1} will be used in calculations involving Fe^{4+}. For Fe^{2+} the isotropic average, calculated with $E \approx 25\,000$ cm^{-1},[16] is $\rho = 0.83$ cm^{-1}, a value which is slightly reduced from the spectroscopic free-ion value, 0.95 ± 0.1 cm^{-1}, deduced by Pryce.[17]

For convenience we define the following energies: (i) $W_1 = \mathcal{E}(^5\hat{B}^a)$, $W_2 = \mathcal{E}(^5\hat{E})$, $W_3 = \mathcal{E}(^5\hat{B}^b)$ for Fe^{2+}; and (ii) $\mathcal{E}_1 = \mathcal{E}(^5\hat{E})$, $\mathcal{E}_2 = \mathcal{E}(^5\hat{B}^a)$, $\mathcal{E}_3 = \mathcal{E}(^5\hat{A})$ for Fe^{4+}. Here $\mathcal{E}(^5\hat{X})$ denotes the energy of the state $^5\hat{X}$ above the respective ground state.

B. Optical transitions and relative intensities

For Fe^{2+} optical transitions from the $^5\hat{A}$ ground state give rise to two electric-dipole-allowed bands in the near ir, $^5\hat{A} \rightarrow {}^5\hat{B}^b$ and $^5\hat{A} \rightarrow {}^5\hat{E}$, which are allowed for $\vec{E} \parallel \vec{c}$ and $\vec{E} \perp \vec{c}$, respectively. For linearly polarized light their intensity ratio is 4:1 (see Fig. 5). Under $\vec{E} \parallel \vec{c}$ the $^5\hat{A} \rightarrow {}^5\hat{B}^b$ band should exhibit three ZPL's, their relative intensities being given by a Boltzmann distribution according to the thermal population of the ground-state levels. Perpendicular transitions to $^5\hat{B}^b$ become weakly allowed via spin-orbit mixing of $^5\hat{E}$ with both $^5\hat{A}$ and $^5\hat{B}^b$. Neglecting the population difference of the ground-state levels the intensity ratio $I_\perp/I_\parallel(^5\hat{A} \rightarrow {}^5\hat{B}^b)$ is found to be

$$\frac{I_\perp}{I_\parallel}(^5\hat{A} \rightarrow {}^5\hat{B}^b) = \frac{13}{24}\left(\frac{3\lambda_2}{\mathcal{E}(^5\hat{E}) - \mathcal{E}(^5\hat{A})}\,\frac{\langle T_2 || \vec{R} || T_2\rangle}{\langle E || \vec{R} || T_2\rangle} + \frac{\lambda_1}{\mathcal{E}(^5\hat{B}^b) - \mathcal{E}(^5\hat{E})}\right)^2. \tag{7}$$

It is certainly a reasonable approximation to assume that the two reduced matrix elements of the dipole operator $\vec{R}$ are equal. This would be correct if all five radial functions were the same. We will not discuss the zero-phonon structure of the $^5\hat{A} \rightarrow {}^5\hat{E}$ band since this transition has not been observed in the experiment.

Because the ground state of Fe^{4+} is $^5\hat{B}^b$ there is only one allowed optical-absorption band $^5\hat{B}^b \rightarrow {}^5\hat{A}$, $^5\hat{B}^b \rightarrow {}^5\hat{B}^a$ being forbidden in first order. This band is complementary to the $^5\hat{A} \rightarrow {}^5\hat{B}^b$ band of Fe^{2+}, its zero-phonon structure is therefore analogous, and the intensity ratio (7) is also valid for it. In second order, transitions to $^5\hat{B}^a$ become allowed for $\vec{E} \perp \vec{c}$ via spin-orbit mixing of $^5\hat{E}$ with both $^5\hat{B}^b$ and $^5\hat{B}^a$. The intensity ratio is given by

$$\frac{I_\perp(^5\hat{B}^b \rightarrow {}^5\hat{B}^a)}{I_\parallel(^5\hat{B}^b \rightarrow {}^5\hat{A})} = \frac{13}{8}\,\frac{\mathcal{E}_2}{\mathcal{E}_3}\left(\frac{\lambda_2}{\mathcal{E}_2 - \mathcal{E}_1}\,\frac{\langle T_2 || \vec{R} || T_2\rangle}{\langle E || \vec{R} || T_2\rangle} + \frac{\lambda_1}{\mathcal{E}_1}\right)^2. \tag{8}$$

C. Spin-Hamiltonian parameters

The effect of second-order spin-orbit and first-order spin-spin interaction on the orbital singlets in Fig. 5 is to split these levels according to the equivalent operator DS_z^2. The spin levels $M_s = 0$, $M_s = \pm 1$, and $M_s = \pm 2$ have therefore relative energies 0, D, and $4D$, respectively. For Fe^{2+} the D parameters are given by

$$D(^5\hat{A}) = \frac{3\lambda_2^2}{\mathcal{E}(^5\hat{E}) - \mathcal{E}(^5\hat{A})} + 3\rho_4\,, \tag{9a}$$

$$D(^5\hat{B}^a) = -\frac{4\lambda_2^2}{\mathcal{E}(^5\hat{B}^b) - \mathcal{E}(^5\hat{B}^a)} + \frac{\lambda_2^2}{\mathcal{E}(^5\hat{E}) - \mathcal{E}(^5\hat{B}^a)} - 3\rho_4\,, \tag{9b}$$

$$D(^5\hat{B}^b) = -\frac{\lambda_1^2}{\mathcal{E}(^5\hat{B}^b) - \mathcal{E}(^5\hat{E})} + \frac{4\lambda_2^2}{\mathcal{E}(^5\hat{B}^b) - \mathcal{E}(^5\hat{B}^a)} - 3\rho_3 . \quad (9c)$$

The same equations apply to the corresponding states of Fe^{4+}.[10] It must be noted, however, that for Fe^{4+} all energy denominators in Eqs. (9) are negative. Since D is of the order 1–10 cm^{-1} for Fe^{2+} and Fe^{4+} the D term is dominant in the $S=2$ spin Hamiltonian. The $M_s=2$ and the $M_s=-2$ spin states are not truly degenerate but are slightly split by higher-order effects. This gives rise to the fourth-order cubic-field term in the $S=2$ spin Hamiltonian. The splitting a has been calculated for the $^5\hat{A}$ ground state of Fe^{2+} to order $\lambda^4, \rho\lambda^2, \rho^2$ and the result is

$$a(^5\hat{A}) = \frac{36\lambda_2^2}{W_2^2}\left(\frac{\lambda_1^2}{W_3} - \frac{\lambda_2^2}{W_1}\right) + \frac{72\rho\lambda_2}{W_2}\left(\frac{\lambda_1}{W_3} - \frac{\lambda_2}{W_1}\right) + 36\rho^2\left(\frac{1}{W_3} - \frac{1}{W_1}\right). \quad (10)$$

Since $|\lambda_1| < |\lambda_2|$ and $W_1 < W_3$, it follows that $a(^5\hat{A}) < 0$ for Fe^{2+}.

The corresponding splitting of the $^5\hat{B}^b$ state of Fe^{4+} is[4]

$$a(^5\hat{B}^b) = 36\left(\frac{\lambda_1}{\mathcal{E}_1}\right)^2\frac{\lambda_2^2}{\mathcal{E}_3} + 36\rho\left(\frac{\lambda_1}{\mathcal{E}_1}\right)^2 + 72\rho\frac{\lambda_1}{\mathcal{E}_1}\frac{\lambda_2}{\mathcal{E}_3} + 36\frac{\rho^2}{\mathcal{E}_3}, \quad (11)$$

and we see that $a(^5\hat{B}^b)$ should be positive. For simplicity we have set $\rho_1=\rho_2=\rho_3=\rho_4=\rho$ in Eqs. (10) and (11). The a parameters turn out to be of the order 0.1–1 cm^{-1}.

The g factors of the $^5\hat{A}$ Fe^{2+} ground state are

$$g_{\parallel} = g_e , \quad (12a)$$

$$g_{\perp} = g_e - 6k_2\lambda_2/W_2 . \quad (12b)$$

If $^5\hat{B}^a$ were the ground state, the g factors would be

$$g_{\parallel} = g_e - 8k_2\lambda_2/W_3 , \quad (13a)$$

$$g_{\perp} = g_e - 2k_2\lambda_2/W_2 . \quad (13b)$$

Note that an accurate measurement of the g factors allows an unequivocal determination of the Fe^{2+} ground state.

For the $^5\hat{B}^b$ ground state of Fe^{4+} the g factors are[4]

$$g_{\parallel} = g_e - 8k_2\lambda_2/\mathcal{E}_2 , \quad (14a)$$

$$g_{\perp} = g_e - 2k_1\lambda_1/\mathcal{E}_1 . \quad (14b)$$

The g shifts $\delta g (= g - g_e)$ in this case are negative while they are positive for Fe^{2+}.

D. Electric dipole intensity of $1 \leftrightarrow -1$ EPR transitions

For $\vec{H} \parallel \vec{c}$ magnetic dipole ($M1$) transitions between the $M_s=1$ and $M_s=-1$ spin levels (Γ_3 and Γ_4 in Fig. 5) are strictly forbidden in S_4 symmetry. On the other hand, electric dipole ($E1$) transitions are allowed if the electric vector of the microwave has a component E_{mw} along H.[18] Such a geometry was present in our 35-GHz experiments where we used a cylindrical cavity operating in the TE_{011} mode. The $E1$ intensity is then proportional to the absolute square of the $E1$ matrix element $\langle\Gamma_3|R_z|\Gamma_4\rangle$. For Fe^{2+} the matrix element $\langle{}^5\hat{A}\Gamma_3|R_z|{}^5\hat{A}\Gamma_4\rangle$ becomes nonzero by spin-orbit mixing of $^5\hat{A}$ with $^5\hat{E}$ in second order and with $^5\hat{B}^b$ in third order. For Fe^{4+} $\langle{}^5\hat{B}^b\Gamma_3|R_z|{}^5\hat{B}^b\Gamma_4\rangle$ becomes nonzero via the mixing of $^5\hat{B}^b$ with $^5\hat{E}$ and $^5\hat{A}$. We find to order λ^4

$$|\langle{}^5\hat{A}\Gamma_3|R_z|{}^5\hat{A}\Gamma_4\rangle|^2 = \frac{9}{2}\left(\frac{\lambda_2}{W_2}\right)^2\left(\frac{3\lambda_2W_3 - 4\lambda_1W_2}{W_2W_3}\right)^2 \times |\langle\psi_r||\vec{R}||\psi_r\rangle|^2_{Fe^{2+}}, \quad (15a)$$

$$|\langle{}^5\hat{B}^b\Gamma_3|R_z|{}^5\hat{B}^b\Gamma_4\rangle|^2 = \frac{9}{2}\left(\frac{\lambda_1}{\mathcal{E}_1}\right)^2\left(\frac{\lambda_1\mathcal{E}_3 - 4\lambda_2\mathcal{E}_1}{\mathcal{E}_1\mathcal{E}_3}\right)^2 \times |\langle\psi_r||\vec{R}||\psi_r\rangle|^2_{Fe^{4+}} . \quad (15b)$$

Here, in analogy to Sec. III B, we have set $\langle T_2||\vec{R}||T_2\rangle = \langle E||\vec{R}||T_2\rangle = \langle\psi_r||\vec{R}||\psi_r\rangle$. The $E1$ oscillator strength now becomes

$$f_{E1} = (4\pi m/\hbar)\nu|\langle\Gamma_3|R_z|\Gamma_4\rangle|^2 , \quad (16)$$

where m is the electron mass and ν is the transition frequency. This has to be compared with the $M1$ oscillator strength of an ordinary $\Delta m = \pm 1$ EPR transition

$$f_{M1} = (h/2mc^2)\nu|\langle\tfrac{1}{2}|S_x|-\tfrac{1}{2}\rangle|^2 . \quad (17)$$

IV. ANALYSIS OF EXPERIMENTAL RESULTS AND INTERPRETATION

A. Fe^{2+}

The two different $S=2$ EPR centers observed in Fe-doped $CdSiP_2$ are assigned to Fe^{2+} and Fe^{4+} substituting for Cd^{2+} and Si^{4+}, respectively. The spectra were analyzed with the following spin Hamiltonian:

$$\mathcal{H} = g_{\parallel}\mu_B H_z S_z + g_{\perp}\mu_B(H_x S_x + H_y S_y) + D(S_z^2 - 2) + \tfrac{1}{120}a(35S_z^4 - 155S_z^2 + 72) + \tfrac{1}{48}a(S_+^4 + S_-^4) + \tfrac{1}{180}F(35S_z^4 - 155S_z^2 + 72) + \sum_{I=1}^{4}\vec{S}\cdot\underline{T}^I\cdot\vec{I}_I , \quad (18)$$

where $S=2$ and z is along the c axis. The last term in (18) represents the ligand hf interaction with the four phosphorus ligands ($I_I = \frac{1}{2}$, 100%).

For Fe^{2+} $g_{\parallel}$ and a are directly obtained from

the $\vec{H}||\vec{c}$ spectrum. An approximate value of D can be inferred from the resonance field of the $1 \longleftrightarrow -1$ transition under $\vec{H}\perp\vec{c}$. If $D \gg g\mu_B H, a, F$ second-order perturbation theory predicts for the resonance condition

$$h\nu = \frac{R-D}{2} + \frac{G_\perp^2}{3D}\left(1+\frac{R+D}{R-D}\right)^{-1}, \tag{19}$$

where $R=(D^2+12G_\perp^2)^{1/2}$ and $G_\perp = g_\perp \mu_B H$. Assuming $g_\perp \approx 2$ yields $D \approx 9.2$ cm^{-1}. The final values of $g_\perp$ and D given in Table I, were obtained from a computer fit to the Fe^{2+} data in Fig. 2 assuming $F=0$. A comparison of the g factors with Eqs. (12) and (13) clearly demonstrates that $^5\hat{A}$ is the ground state. While the sign of a could be determined from the cubic anisotropy of the $1 \longleftrightarrow -1$ transition under $\vec{H}\perp\vec{c}$ the sign of D was not determined experimentally. It is however obvious from Eq. (9a) that $D(^5\hat{A})$ must be positive.

The $^5\hat{A} \rightarrow {}^5\hat{B}^b$ optical transition of Fe^{2+} is expected to induce the most prominent absorption band in the near ir. Therefore we have ascribed the 1.8-μm band (Fig. 4) to this transition. This assignment is fully consistent with the observed polarization of the band and its zero phonon structure. Correlating the position of the hot bands with $D(^5\hat{A}) = 9.9$ cm^{-1}, yields

$$D(^5\hat{B}^b) = +0.8 \pm 0.6 \text{ cm}^{-1} \text{ for } Fe^{2+}.$$

The failure to observe transitions to the levels of $^5\hat{E}$ is not clear. It is possible that they are masked by strong water vapor absorption between 2.5 and 2.7 μm or that they occur beyond 3.0 μm.

To estimate W_1 and W_2 we proceed as follows: With the parameters of Sec. III A, Eq. (12b) predicts $W_2 \approx 4000$ cm^{-1}. This value can be checked by comparing the theoretical value of $D(^5\hat{A})$ [Eq. (9a)] with the measured one. One finds $D(^5\hat{A}) = 10.3$ cm^{-1} in good agreement with experiment (9.9 cm^{-1}). From Eq. (9c) and $D(^5\hat{B}^b) = 0.8$ cm^{-1} it follows that $W_3 - W_1 \approx 4270$ cm^{-1}. With $W_3 = 5340$ cm^{-1} from the optical spectrum, this gives $W_1 \approx 1070$ cm^{-1}. These values correspond to the crystal-field parameters Dq, μ, δ given in Table IV. We note that for Fe^{2+} in GaP,[19] Dq is about 380 cm^{-1} which is very close to the present value. It is now possible to calculate $a(^5A)$ from Eq. (10) and the result is -0.33 cm^{-1} as compared to the experimental value of -0.60 cm^{-1}. In view of the fact that a is a fourth-order effect of H_{so} and a second-order effect of H_{ss} this is a reasonable result. From Eq. (7) we finally infer that $(I_\perp/I_\parallel)(^5\hat{A} \rightarrow {}^5\hat{B}^b) \approx 0.01$ which explains why we did not observe any ZPL in the $^5\hat{A} \rightarrow {}^5\hat{B}^b$ band for $\vec{E}\perp\vec{c}$.

TABLE IV. Crystal-field parameters of Fe^{2+} and Fe^{4+} in $CdSiP_2$ (in cm^{-1}).

	Dq	μ	δ
Fe^{2+}	390	−1070	−1350
Fe^{4+}	≈ 810	≈ 800	1100

B. Fe^{4+}

A computer fit to the Fe^{4+} EPR data in Fig. 2 allows the determination of $g_\parallel$, $g_\perp$, D, and $(a+\frac{2}{3}F)$. From the cubic anisotropy of the $-1 \longleftrightarrow 1$ transition under $\vec{H}\perp\vec{c}$ one obtains a separately. However, since the anisotropy is smaller than the linewidth, this value is not very accurate. Again the sign of D cannot be determined from our EPR data alone but the correlation with the optical results implies $D(^5\hat{B}^b) > 0$ as will be shown below.

The weak absorption band near 1.1 μm is ascribed to the $^5\hat{B}^b \rightarrow {}^5\hat{A}$ transition of Fe^{4+}. This assignment is suggested by the fact that the band is only visible for $\vec{E}||\vec{c}$ in analogy to the $^5\hat{A} \rightarrow {}^5\hat{B}^b$ band of Fe^{2+}. From Eqs. (7) and (8) we see that $\vec{E}\perp\vec{c}$ transitions to $^5\hat{A}$ and $^5\hat{B}^a$ are two orders of magnitude weaker than $\vec{E}||\vec{c}$ transitions to $^5\hat{A}$. In our crystals these transitions are therefore beyond the detection limit. The evaluation of the ZPL's in the $^5\hat{B}^b \rightarrow {}^5\hat{A}$ band is complicated by the facts that one cannot decide about the sign of $D(^5\hat{B}^b)$ from Eq. (9c) and that only one hot band is observed. According to Eq. (9a) we can however assume that $D(^5\hat{A})$ is negative. Then, there is only one possibility which does not lead to contradictions: (i) $D(^5\hat{B}^b) > 0$; (ii) the 9264.2-cm^{-1} ZPL and the 9258.8-cm^{-1} hot ZPL have to be assigned to the transitions $\Gamma_2(^5\hat{B}^b) \rightarrow \Gamma_1(^5\hat{A})$ and $\Gamma_{3+4}(^5\hat{B}^b) \rightarrow \Gamma_{3+4}(^5\hat{A})$, respectively. This implied

$$D(^5\hat{A}) = -3.6 \pm 0.8 \text{ cm}^{-1} \text{ for } Fe^{4+}.$$

It is not possible to obtain $\mathcal{E}_2$ directly from the present data. However $\mathcal{E}_2 \approx 8500$ cm^{-1} should be a reasonable value. Equation (9c) together with $D(^5\hat{B}^b) = 1.8$ cm^{-1} gives $\mathcal{E}_1 \approx 1100$ cm^{-1}. Equation (9a) then predicts $D(^5\hat{A}) = -2.8$ cm^{-1}, which is only slightly smaller than the experimental value above. With $\mathcal{E}_3 = 9260$ cm^{-1} from the 1.1-μm band, we finally obtain Dq, δ, and μ as given in Table IV.

If one calculates $\delta g_\parallel$ and $\delta g_\perp$ from Eqs. (14a) and (14b) one finds values which are too large by factors of ~4 and ~30, respectively. Similarly $a(^5\hat{B}^b)$ as calculated from Eq. (11) is about 40 times too large and has the wrong sign. Primarily, this is believed to be the result of covalent effects beyond those contained in the ligand field model of Vallin and Watkins,[4] e.g., excitations to charge transfer states. Experimentally it is known[20] that these effects become progressively more important

the higher the charge state of the metal ion. In $SrTiO_3$ the effect is so large that a positive g shift results for Fe^{4+}.[20] This is also obvious from the present work. The g factors of the isoelectronic $3d^5$ ions Cr^+, Mn^{2+}, and Fe^{3+} in $CdSiP_2$ are 1.998, 2.004,[21] and 2.036, respectively. The increase in g clearly demonstrates the increasing importance of covalency effects the higher the charge state[22,23] of the ion. In the present case Jahn-Teller effects should play a minor role in modifying the g shifts and the fourth-order cubic splitting a, since they all arise from higher-order perturbations. Therefore, a strong reduction of spin-orbit or Zeeman interaction due to the Ham effect[24] cannot occur unless the static tetragonal splitting is small compared with the energy of the vibrational mode involved in the Jahn-Teller coupling. This cannot be the case for Fe^{4+} in $CdSiP_2$ where $\delta \approx 1100$ cm^{-1}.

C. Fe^+ and Fe^{3+}

Fe^+ has the configuration d^7 and a tetrahedral field leaves an orbital singlet $^4A_2$ lowest. Under the combined action of tetragonal field and spin-orbit interaction this level splits into two Kramers doublets $\pm\frac{1}{2}$ and $\pm\frac{3}{2}$ with a zero-field splitting $2D$. The Fe^+ EPR spectrum was analyzed with the conventional $S=\frac{3}{2}$ spin Hamiltonian. The effective $g_\perp$ factor of the $\pm\frac{1}{2}$ doublet, $g'_\perp = 4.379$, was identical at 9.5 and 34.8 GHz, thus indicating that $|2D| > 10$ cm^{-1}. This situation is analogous to Co^{2+} and Ni^{3+} in I_B-III-S_2 compounds.[25] The g factors, were evaluated with the help of the expressions

$$g_\parallel = g_e - 8k_2\lambda_2/\mathcal{E}(^4\hat{B}), \tag{20a}$$

$$g_\perp = g_e - 8k_2\lambda_2/\mathcal{E}(^4\hat{E}), \tag{20b}$$

$$2D = 8\lambda_2^2[1/\mathcal{E}(^4\hat{E}) - 1/\mathcal{E}(^4\hat{B})], \tag{21}$$

where $^4\hat{B}$ and $^4\hat{E}$ are the split-off levels of the first excited cubic $^4T_2$ state. Inserting k_2 and λ_2 from Table III into Eqs. (20a) and (20b) yields $\mathcal{E}(^4\hat{B}) \approx 7240$ cm^{-1} and $\mathcal{E}(^4\hat{E}) \approx 3715$ cm^{-1} corresponding to $Dq \approx 490$ cm^{-1} and a tetragonal splitting of $^4T_2$ of about 3500 cm^{-1}. With these values Eq. (21) predicts $2D \approx 14$ cm^{-1}. The observed g factor of Fe^+ in GaP is $g = 2.131$.[26] Using λ_2, k_2, and Dq from above, the predicted g factor for Fe^+ in GaP is 2.143. Our estimates for λ_2, k_2, and Dq thus appear to be reasonable.

The Fe^{3+} spectrum was analyzed with the usual spin Hamiltonian[27] for the ^6S ground state of $3d^5$ in tetragonal symmetry. The effective g factors of the $\pm\frac{1}{2}$ doublet are $g_\parallel = 2.036$ and $g_\perp = 5.613$. From the observed $\pm\frac{1}{2} \leftrightarrow \pm\frac{3}{2}$ transition one then obtains $|2D - \frac{5}{2}(a + \frac{2}{3}F)| = 1.972$ cm^{-1}. It is not possible to determine $a + \frac{2}{3}F$ separately since additional allowed fine-structure lines were not observed. A typical value of $a + \frac{2}{3}F$ for Fe^{3+} in similar systems is 0.01 cm^{-1} and the error limit quoted for $|D|$ in Table II refers to this quantity. A direct check for this interpretation is available since[28]:

$$g'_\perp = 3g_\perp[1 - \tfrac{2}{9}(h\nu/2D)^2]. \tag{22}$$

With $g_\perp \approx g_\parallel$ and $2D$ from Table II we calculate $g'_\perp = 5.638$ in good agreement with the experimental result. D values of the order 1 cm^{-1} are usually only found for $3d^5$ ions associated with some other defect. No evidence for defect association could be found in the present case indicating that charge compensation is remote. For an isolated Fe^{3+} ion $D \approx 1$ cm^{-1} is exceptionally large.

For Fe^{3+} in GaP phosphorus ligand hf structure has not been resolved, probably because of the presence of Ga^{69}, Ga^{71}($I=\frac{3}{2}$, 100%), and/or strain broadening.[21] The ligand hf splitting for $\vec{H} \parallel [001]$, T_{001}, can however be inferred from electron-nuclear double-resonance data of Teuerle *et al.*[29] One finds for GaP, $T_{001} = 8.7\times10^{-4}$ cm^{-1}. The slightly larger EPR value (Table II) observed for $CdSiP_2$ is possibly due to the fact that the bond distance in GaP(2.360 Å) is slightly larger than the Si–P bond (2.247 Å) in $CdSiP_2$.

The small reduction in Fe^{2+} and Fe^{4+} EPR intensity upon uv irradiation appears to be correlated with the creation of Fe^+ and Fe^{3+}, thus suggesting that small percentages of Fe^{2+} and Fe^{4+} are converted into Fe^+ and Fe^{3+}, respectively, by the trapping of photoelectrons. The quenching of Fe^+ and Fe^{3+} by ir irradiation is thought to be associated with the release of trapped holes which are retrapped by Fe^+ and Fe^{3+}.

V. DISCUSSION

A. $E1$ intensity of $1 \leftrightarrow -1$ EPR transitions

It has been shown in Sec. III D that the residual intensity of the Fe^{2+} $1 \leftrightarrow -1$ transition for $\vec{H} \parallel \vec{c}$ must be of $E1$ origin if the symmetry is purely tetragonal. Since we could not find any indication for a deviation from tetragonal symmetry we believe that this residual intensity is indeed of $E1$ origin. This is also consistent with the following estimate. Taking $|\langle E\|\vec{R}\|T_2\rangle|^2 = 0.024$ Å^2, a value appropriate for Fe^{2+} in ZnS,[30] $\nu = 35$ GHz, and allowing for a 20% uncertainty in λ_1, Eqs. (15a) and (16) predict for the $E1$ oscillator strength $f_{E1}(Fe^{2+}) \approx 0.9\times10^{-12}$. This is only one order of magnitude smaller than the $M1$ oscillator strength [Eq. (17)] of an ordinary allowed EPR transition. Since we estimate the Fe^{2+} concentration to be 100–1000 ppm in our doped crystals it is in fact possible to observe $E1$ transitions of Fe^{2+}. On the other hand, we can also understand the vanishing

TABLE V. Second- and fourth-order axial-field parameters of $3d$ ions in chalcopyrite compounds (in cm^{-1}).

	Fe^{2+} $CdSiP_2$	Fe^{4+} $CdSiP_2$	$CuAlS_2$	Ni^{+} $CuGaS_2$	$AgGaS_2$	Ti^{3+} $CuAlS_2$	Fe^{2+} $CuAlS_2$
Ds	346	≈271	190	197	430	<−72	−243
Dt	52	≈48	57	49	89	>−48	−29
Dt/Ds [a]	0.15	≈0.18	0.30	0.25	0.21	<0.66	0.12
	(0.051)	(0.041)	(0.071)	(0.069)	(0.058)	(0.077)	(0.067)

[a] Values in parentheses are calculated from Eq. (24).

$E1$ intensity of the corresponding Fe^{4+} line at $\vec{H} \parallel \vec{c}$. Taking $\lambda_1/\mathcal{E}_1 \approx 0.005$ as inferred from $g_{\parallel}$, λ_1, and λ_2 from Table III, and the same reduced $E1$ matrix element as for Fe^{2+}, we have from Eqs. (15b) and (16) $f_{E1}(Fe^{4+}) \approx 0.3 \times 10^{-12}$. According to the optical results the Fe^{4+} concentration is at least one order of magnitude smaller than that of Fe^{2+}, whence it follows that the $E1$ intensity of Fe^{4+} is probably below the detection limit.

B. Site inequivalence

For each type of metal ion in a chalcopyrite-structure compound there are two inequivalent sites in the unit cell which result from the clockwise and counterclockwise rotation of the anion tetrahedra around the c axis.[31] For EPR centers with $S \geq 2$ this leads to a splitting of EPR lines via the fourth-order cubic term in the spin Hamiltonian as has been demonstrated for $CuGaS_2$:Fe^{3+} (Ref. 27) and Mn^{2+} in II_B-IV-V_2 compounds.[21] In the present cases this splitting was too small to be resolved. However, the inequivalence of the two Si sites in $CdSiP_2$, for which Fe^{4+} probably substitutes, manifests via the anisotropy of the ligand hf splitting which must be responsible for the peculiar shape variation of the $1 \leftrightarrow -1$ line under $\vec{H} \perp \vec{c}$, see Sec. II A.

C. Axial-field parameters in chalcopyrite compounds

For Fe^{2+} and Fe^{4+} the second- and fourth-order axial-field parameters, Ds and Dt, can be evaluated from the experimental axial-field splittings δ and μ according to[10]

$$Ds = \mp\tfrac{1}{7}(\mu + \delta), \quad Dt = \pm\tfrac{1}{14}(\mu - \tfrac{4}{3}\delta), \tag{23}$$

where the upper signs apply to d^1 and d^6 and the lower ones to d^4 and d^9. These parameters together with the ratio Dt/Ds are listed in Table V. For comparison we have also included the corresponding values for $Ni^{+}(d^9)$ in $CuAlS_2$, $CuGaS_2$, $AgGaS_2$,[14] $Ti^{3+}(d^1)$ in $CuAlS_2$,[32] and Fe^{2+} in $CuAlS_2$.[33] It is evident that the largest values occur for $AgGaS_2$ and $CdSiP_2$ which have the largest tetragonal distortion of all ternary chalcopyrite compounds.[1]

Considering only the nearest neighbors, the point-ion model predicts

$$\frac{Dt}{Ds} = \frac{10}{27}\,\frac{\langle r^4 \rangle}{d^2 \langle r^2 \rangle}, \tag{24}$$

where d is the nearest-neighbor distance. Values of Dt/Ds calculated from Eq. (24) with the free-ion radial averages listed in Ref. 12 and the distances given in Refs. 34 and 35 are also included in Table V. The calculated values have the correct sign and the correct order of magnitude but are uniformly too small. This is not surprising in view of the inherent limitations of the point-charge model and of the fact that Eq. (24) does not contain contributions of more distant ligand shells to Ds and Dt.

VI. SUMMARY

An EPR analysis reveals that Fe impurities in $CdSiP_2$ can exist in four different charge states, Fe^{+}, Fe^{2+}, Fe^{3+}, and Fe^{4+}. Energetically and thermally the most stable states are Fe^{2+} and Fe^{4+} substituting for Cd^{2+} and Si^{4+}, respectively. Both Fe^{2+} and Fe^{4+} can trap photoelectrons thus being converted into Fe^{+} and Fe^{3+}. With respect to the lattice these ions are then negatively charged and therefore attract holes which are released from some other, more shallow traps by ir irradiation or thermal excitation. The relative intensity of the near ir absorption bands of Fe^{2+} and Fe^{4+} indicates that the Fe^{2+} concentration is at least an order of magnitude larger than that of Fe^{4+}. The intensity changes in the EPR spectra upon irradiation show that the Fe^{+} and Fe^{3+} concentrations are only a few percent of the Fe^{2+} and Fe^{4+} concentrations, respectively.

The EPR and optical results were analyzed in the framework of crystal-field theory supplemented to include covalency effects as in the treatment of Vallin and Watkins.[4] Static crystal-field theory satisfactorily accounts for all experimental details except for the Fe^{4+} EPR data. We suggest that the discrepancies encountered in this case are due to covalent effects not contained in the ligand field model of Vallin and Watkins.

ACKNOWLEDGMENTS

I am grateful to Dr. P. Koidl, Dr. A. Räuber, and Professor J. Schneider for helpful discussions, to Dr. B. Dischler and Dr. R. Röhrig for permission to use their EPR computer program, to Dr. F. S. Ham and Professor G. D. Watkins for a valuable correspondence, to R. Moritz for growing Fe-doped $CdSiP_2$, and to K. Sambeth for expert technical assistance.

[1]J. L. Shay and J. H. Wernick, *Ternary Chalcopyrite Semiconductors—Growth, Electronic Properties, and Applications* (Pergamon, New York, 1975).
[2]T. Teranishi, K. Sato, and K. Kondo J. Phys. Soc. Jpn. 36, 1618 (1974).
[3]E. Ziegler, W. Siegel, and G. Kühnel, Phys. Status Solidi A 18, 483 (1973).
[4]J. T. Vallin and G. D. Watkins, Phys. Rev. B 9, 2051 (1974).
[5]K. Leutwein, Appl. Opt. 10, 46 (1971).
[6]We use Mullikan's notation and that of G. F. Koster, J. O. Dimmock, R. G. Wheeler, and H. Statz [*Properties of the 32 Point groups* (MIT, Cambridge, 1963)] to denote the transformation properties of orbital states and of spin-orbit states, respectively. The orbital states in S_4 symmetry are labeled with carets.
[7]G. F. Koster, J. O. Dimmock, R. G. Wheeler and H. Statz, in Ref. 6.
[8]J. Dieleman, R. S. Title, and W. V. Smith, Phys. Lett. 1, 334 (1962).
[9]M. Bettini, W. Bauhofer, M. Cardona, and R. Nitsche, Phys. Status Solidi B 63, 641 (1974).
[10]J. T. Vallin, G. A. Slack, S. Roberts, and A. E. Hughes, Phys. Rev. B 2, 4313 (1970).
[11]With this sign convention for μ and δ the point-ion model predicts positive values for d^4 and d^9 and negative values for d^1 and d^6 if the anion tetrahedron is compressed along c. The signs are reversed for an elongated tetrahedron. This rule is in fact obeyed for Ti^{3+} (Ref. 32) and Fe^{2+} (Ref. 33) in $CuAlS_2$, Ni^+ in I_B-III-S_2 compounds (Ref. 14) and Fe^{2+} in $CdSiP_2$.
[12]A. Abragam and B. Bleaney, *Electron Paramagnetic Resonance of Transition Ions* (Oxford U.P., London, 1970).
[13]R. E. Trees, Phys. Rev. 82, 683 (1951).
[14]U. Kaufmann, Phys. Rev. B 11, 2478 (1975).
[15]The spin-orbit contribution to ρ_4 has been calculated by the method outlined in Ref. 4.
[16]C. E. Moore, Natl. Bur. Stds. Circular No. 467 (U.S. GPO, Washington, D.C. 1971).
[17]M. H. L. Pryce, Phys. Rev. 80, 1107 (1950).
[18]Since the z component of the $E1$ operator $\vec{R}$ transforms as Γ_2 in S_4 this statement follows from the fact that $\Gamma_3^* \times \Gamma_2 \times \Gamma_4 = \Gamma_1$.
[19]J. M. Baranowski, J. W. Allen, and G. L. Pearson, Phys. Rev. 160, 627 (1967).
[20]O. F. Schirmer, W. Berlinger, and K. A. Müller, Solid State Commun. 16, 1289 (1975).
[21]U. Kaufmann, A. Räuber, and J. Schneider, Phys. Status Solidi B 74, 169 (1976).
[22]I. Fidone and K. W. H. Stevens, Proc. Phys. Soc. Lond. 73, 116 (1959).
[23]H. Watanabe, J. Phys. Chem. Solids 25, 1471 (1964).
[24]F. S. Ham, Phys. Rev. 138, A1727 (1965).
[25]U. Kaufmann, A. Räuber, and J. Schneider, Solid State Commun. 15, 1881 (1974).
[26]Ken Suto and Jun-ichi Nishizawa, J. Phys. Soc. Jpn. 27, 924 (1969).
[27]J. Schneider, A. Räuber, and G. Brandt, J. Phys. Chem. Solids 34, 443 (1974).
[28]G. W. Ludwig and H. H. Woodbury, in *Solid State Physics*, edited by F. Seitz, D. Turnbull, and H. Ehrenreich (Academic, New York, 1962), Vol. 13.
[29]W. Teuerle, E. Blaschke, and A. Hausmann, Z. Phys. 270, 37 (1974).
[30]G. A. Slack, F. S. Ham, and R. M. Chrenko, Phys. Rev. 152, 376 (1966).
[31]U. Kaufmann and J. Schneider, in *Festkörperprobleme XIV-Advances in Solid State Physics*, edited by H. J. Queisser (Vieweg-Pergamon, Braunschweig, 1974).
[32]U. Kaufmann, A. Räuber, and J. Schneider, J. Phys. C 8, L381 (1975).
[33]U. Kaufmann, Solid State Commun. 19, 213 (1976).
[34]M. D. Lind and R. W. Grant, J. Chem. Phys. 58, 357 (1973).
[35]G. Brandt, A. Räuber, and J. Schneider, Solid State Commun. 12, 481 (1973).